mater.scichina.com link.springer.com

Sci China Mater 2025, 68(3): 860–867
https://doi.org/10.1007/s40843-024-3252-3

SPECIAL ISSUE: 2025 Emerging Investigator Issue

Tailoring small-molecule acceptors through asymmetric side-chain substitution for efficient organic solar cells

Lan Xie[1,2†], Dingding Qiu[3†], Xianghao Zeng[2], Chung Hang Kwok[2], Yan Wang[2], Jia Yao[2], Kan Ding[4], Lu Chen[2], Jicheng Yi[2], Harald Ade[4], Zhixiang Wei[3], Wai-Yeung Wong[1*], He Yan[2*] and Han Yu[1,2*]

ABSTRACT **Side chain engineering of small-molecule acceptors (SMAs) is a promising strategy for improving device efficiency in organic solar cells (OSCs). This study investigates the parent SMAs of BT-BO and BT-TBO, along with the newly synthesized asymmetric SMA, BT-ASY, which features branched alkyl chains and thiophene side chains substituted at the β positions of the thiophene units, respectively. Despite exhibiting comparable optical and electrochemical properties, the PM6:BT-ASY-based device achieves a power conversion efficiency (PCE) of 18.08% representing a significant improvement over its symmetric counterparts. This enhancement is primarily attributed to improved charge mobility, extended carrier lifetimes, optimized molecular packing, and effective phase separation, as confirmed by grazing incidence wide-angle X-ray scattering measurements. Our findings highlight that asymmetric side-chain strategy enhances π-π stacking and electronic coupling, offering a simple yet effective approach to improving photovoltaic performance. This work underscores the potential of asymmetric structural modifications in SMAs for advancing OSC technology and renewable energy solutions.**

Keywords: organic solar cells, side chain engineering, active layer, asymmetric acceptors, thiophene side chains

INTRODUCTION

Organic solar cells (OSCs) are widely researched due to their potential of low-cost production, flexibility, lightweight properties, and the ability to be tailored for specific applications, which makes them promising candidates for sustainable energy solutions [1–3]. In OSCs, the photoactive layer is typically composed of p-type donor polymers (e.g., PM6) and n-type small-molecule acceptors (SMAs), determining the light absorption and power conversion efficiencies (PCEs) of devices [4–8]. Recent breakthroughs have propelled OSCs with PCEs surpassing 20% [9–11], primarily due to the development of SMAs featuring crescent-shaped architecture like Y6 [12]. Although numerous derivatives based on the Y6 structure have been developed, achieving remarkable progress, a clear and effective understanding of the structure-property relationships remains lacking, which poses significant challenges for the optimization of OSC devices and further enhancement of performance [12–22].

Numerous studies have focused on optimizing the branching points, dimensions, length, and shape of alkyl chains in SMAs [23–31]. Side-chain engineering, including variations in branching points, size, length, and shape, is crucial alongside tuning the end groups and central core [32,33]. Substituents with aromatic groups (e.g., phenyl or thiophenyl) offer superior packing and charge transport properties compared to conventional saturated alkyl chains, leading to record-breaking efficiencies [34,35]. Additionally, introducing asymmetric side chains combines the advantages of different configurations, effectively fine-tuning the packing morphology and optoelectronic properties of materials, ultimately enhancing photovoltaic performance [35–37]. In the realm of organic photovoltaics, thiophene is frequently utilized in the development of high-performance polymer donors like PM6 and D18, but few works demonstrate their impact as side chains in SMAs [38]. As for the building block with side chain substitution in Y-series SMAs, the β-positions of thiophene units are crucial for optimizing molecular stacking and electronic interactions. Previous studies have shown that even minor modifications to thiophene can significantly impact the morphological and optoelectronic characteristics of these materials, leading to notable variations in performance [39–42]. Currently, there is a lack of systematic studies examining the impact of β-position modifications of thiophene side chains with asymmetric strategy on the performance of the SMAs [25,36,43–45]. Thus, investigating the intramolecular and intermolecular dynamics of SMAs with asymmetric side chains of alkyl and thiophene chains could provide valuable correlations between fundamental properties and overall device performance [46–49].

[1] Department of Applied Biology and Chemical Technology and Research Institute for Smart Energy, The Hong Kong Polytechnic University, Hong Kong 999077, China
[2] Department of Chemistry and Hong Kong Branch of Chinese National Engineering Research Center for Tissue Restoration and Reconstruction, Hong Kong University of Science and Technology, Hong Kong 999077, China
[3] CAS Key Laboratory of Nanosystem and Hierarchical Fabrication National Center for Nanoscience and Technology, Beijing 100190, China
[4] Department of Physics and Organic and Carbon Electronics Laboratories (ORaCEL), North Carolina State University, Raleigh, NC 27695, USA
† Equally contributed to this work.
* Corresponding author (email: wai-yeung.wong@polyu.edu.hk; hyan@ust.hk; yuhan.yu@polyu.edu.hk)

In this study, we systematically explore the impact of asymmetric versus symmetric side chains on the physicochemical properties, and OSCs performance of SMAs. Based on the high-efficiency SMA, BT-BO (with symmetric alky chains), and its derivative BT-TBO (with symmetric thiophene chain), we developed a new asymmetric SMA, BT-ASY, with asymmetric alkyl chain and thiophene chain substitution, respectively, shown in Fig. 1a. The three SMAs display comparable optical properties, with molecular energy levels increasing progressively from BT-BO to BT-ASY and finally to BT-TBO. BT-ASY shows improved molecular stacking along the conjugated backbones, as confirmed by grazing incidence wide-angle X-ray scattering (GIWAXS) measurements, resulting in enhanced electron mobility in both neat acceptor films and donor-acceptor (D-A) blend films. The higher PCE observed in the PM6:BT-ASY device (PCE = 18.08%, short-circuit current density (J_{SC}) = 27.15 mA cm^{-2}, V_{OC} = 0.849 V, and fill factor (FF) = 78.44%), which can be attributed to BT-ASY's superior charge transport capabilities, enhanced molecular interactions, and suitable phase separation. Overall, our results indicate that the asymmetric side-chain strategy is an effective approach for fine-tuning photoelectric properties and improving the photovoltaic performance of OSCs.

EXPERIMENTAL SECTION

The synthesis of BT-ASY is outlined in Scheme S1 (available in the Supporting Information), with detailed procedures provided in the same section. The key intermediate, compound **2**, was synthesized through a $Pd(PPh_3)_4$-catalyzed Stille coupling reaction using two different organotin compounds, achieving a yield of 40%. Following this, an intramolecular Cadogan reductive cyclization with PPh_3 and *N*-alkylation with 2-ethylhexyl were performed to create a central core with asymmetric alkyl side chains (compound **3**). Compound **3** then underwent a Vilsmeier-Haack reaction, followed by a Knoevenagel condensation, resulting in the target molecule BT-ASY. It is noteworthy that the synthesis of BT-ASY involves the same number of steps as the symmetric compounds BT-BO and BT-TBO. we utilized two different organotin reagents to achieve an asymmetric coupling product (compound **2**) via a one-pot method. The chemical structures of the intermediates and final products were confirmed using ^{1}H NMR, ^{13}C NMR, and MALDI-TOF techniques.

RESULTS AND DISCUSSION

Optical and electrochemical properties

The absorption spectra of BT-BO, BT-TBO, and BT-ASY in chloroform (CF) solutions and the solid state are presented in Fig. 1c, d, with corresponding optical parameters summarized in Table 1. In solution, the three SMAs exhibit nearly identical spectra, with maximum absorption wavelengths (λ_{max}) at 730 nm for BT-BO, 731 nm for BT-ASY, and 732 nm for BT-TBO. This indicates that altering the side chains of Y6-like SMAs has minimal impact on the intramolecular charge transfer (ICT) effect [50,51]. When transitioning from solution to solid films, BT-BO and BT-ASY show similar redshifts of 69 and 72 nm, respectively, compared to a more significant redshift of 86 nm for BT-TBO. These differences are attributed to the unique

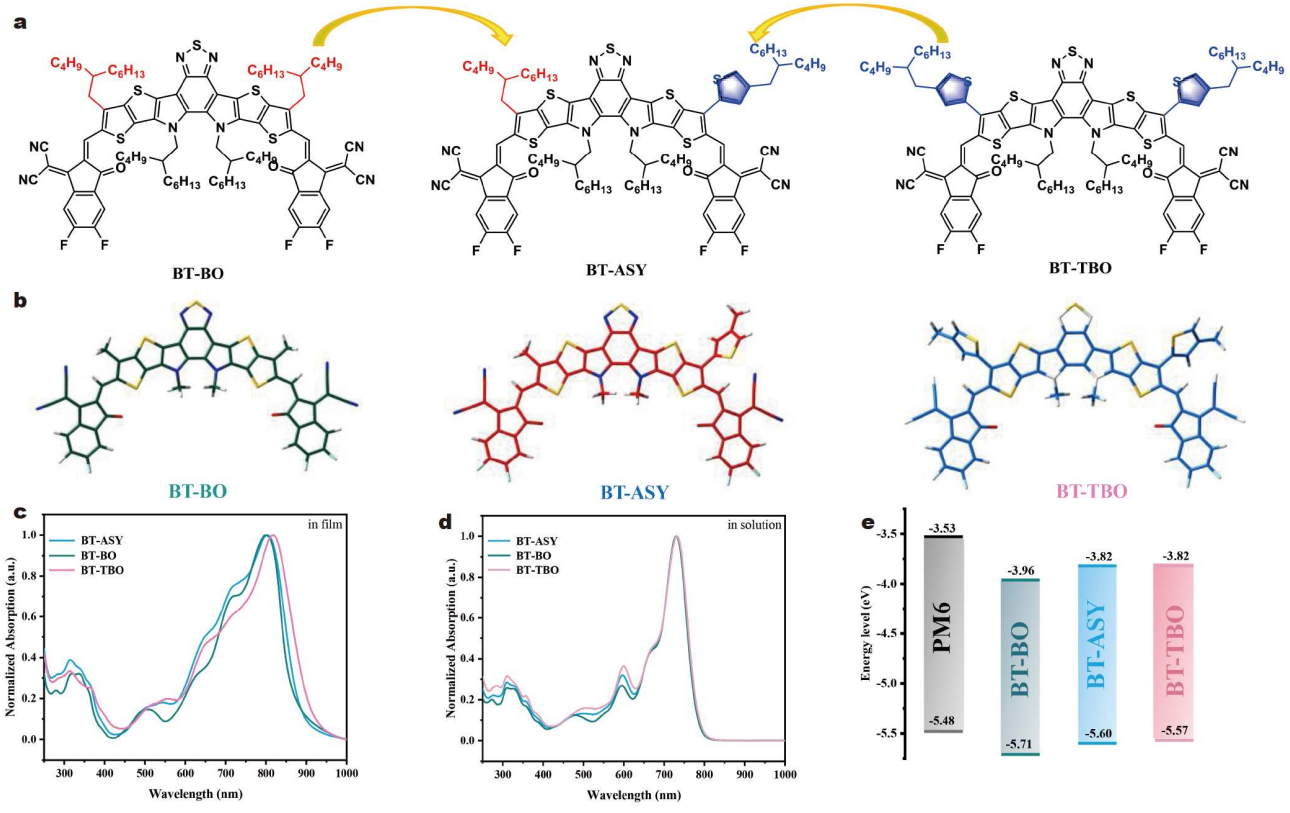

Figure 1 (a) Molecular structures of BT-BO, BT-TBO, and BT-ASY. (b) The monomolecular single crystallographic structures in the top-view of BT-BO, BT-TBO, and BT-ASY. Absorption spectra of BT-BO, BT-TBO, and BT-ASY (c) in the thin-film state, and (d) in dilute chloroform solutions. (e) Energy level diagrams of PM6, BT-BO, BT-TBO, and BT-ASY in thin films.

Table 1 Optical and electrochemical parameters of BT-BO, BT-TBO, and BT-ASY

Acceptor	λ_{max}^{sol} (nm)	λ_{max}^{film} (nm)	λ_{onset}^{film} (nm)	E_g^{opt} (eV)[a]	$LUMO^{CV}$ (eV)	$HOMO^{CV}$ (eV)	$LUMO^{DFT}$ (eV)	$HOMO^{DFT}$ (eV)
BT-BO	730	800	873	1.42	−3.96	−5.71	−3.50	−5.61
BT-ASY	731	803	898	1.38	−3.81	−5.60	−3.49	−5.53
BT-TBO	732	817	922	1.34	−3.82	−5.57	−3.49	−5.56

a) Calculated from $E_g^{opt} = 1240/\lambda_{onset}$.

aggregation behaviors of the three SMAs in the solid state. The optical bandgaps for BT-BO, BT-TBO, and BT-ASY were estimated to be 1.42, 1.34, and 1.38 eV, respectively, based on the absorption edge onset, determined by the intersection of the tangent to the peak absorption edge with the vertical axis (Y = 0).

The molecular energy levels of these acceptors were assessed using cyclic voltammetry (CV) (Fig. 1e). The lowest unoccupied molecular orbital (LUMO) and highest occupied molecular orbital (HOMO) values are −3.96/−5.71 eV for BT-BO, −3.81/−5.60 eV for BT-ASY, and −3.82/−5.57 eV for BT-TBO. The slightly elevated LUMO values for BT-ASY, and BT-TBO compared with BT-BO, can be associated with the weak electron-donating properties of thiophene, which contributes to achieving a higher V_{OC} in the resulting devices. Density functional theory (DFT) calculations were performed at the B3LYP/6-31G(d,p) level to understand the molecular structure properties of these NFAs. For simplicity of the calculations, all the alkyl chains of the four NFAs were substituted with methyl groups. From the optimized geometries (Fig. 1b) and Table 1, the LUMO and HOMO values are −3.50/−5.61 eV for BT-BO, −3.49/−5.53 eV for BT-ASY, and −3.49/−5.62 eV for BT-TBO. The results from DFT calculations are consistent with those from CV. As we progress from a side chain without thiophene to an asymmetric structure with one thiophene, and then to a small molecule acceptor (SMA) with two thiophene side chains, the HOMO levels continuously decrease while the LUMO levels increase slightly. This indicates that the introduction of thiophene side chains can effectively regulate molecular energy levels.

Performance characterization

To investigate the impact of asymmetric side chains on cell efficiency, we prepared conventional binary OSCs with the conventional architecture ITO glass/PEDOT: PSS/PM6/PNDIT-F3N/Ag. The polymer PM6, a commonly used commercial donor was selected as the donor in the active layer due to its deep HOMO energy level and complementary absorption spectra with the three acceptors. The best J-V curves and corresponding external quantum efficiency (EQE) spectra are presented in Fig. 2a, b. As shown in Table 2, increasing the number of thiophene-based side chains in the SMAs leads to a gradual decrease in V_{OC}, with values of 0.865 V for BT-BO and 0.849 V for BT-ASY, and 0.828 V for BT-TBO. This trend aligns with the differing LUMO values. Notably, the asymmetric BT-ASY-based device achieves an impressive PCE of 18.08%, accompanied by an outstanding FF of 78.44% and a respectable short-circuit current density (J_{SC}) of 27.15 mA cm^{-2}, which are higher than those of the symmetric acceptor-based devices (PM6:BT-BO, PCE = 15.27%, J_{SC} = 24.04 mA cm^{-2}, FF = 73.46%; PM6:BT-TBO, PCE = 17.21%, J_{SC} = 26.90 mA cm^{-2}, FF = 77.27%). The enhanced J_{SC} and FF of the BT-ASY-based device are attributed to the improved molecular stacking and superior charge transport capabilities in the active layer. Fig. 2b shows that both optimal cells exhibit strong, broad photovoltaic responses in the wavelength range of 500 to 900 nm. The superior EQE response in the PM6: BT-ASY device is likely due to its more favorable morphology compared to the PM6: BT-BO, and PM6: BT-TBO blends. The integrated J_{SC} value of 26.51 mA cm^{-2} from the EQE spectra in the PM6:BT-ASY device further confirms the reliability of the device data.

Next, we plotted the curves of J_{SC} or V_{OC} against different light intensities (P_{light}) to analyze charge recombination behaviors. As shown in Fig. 2d, e, and the parameters shown in Table S1, all devices exhibited a similar slope (A) of ~1 in the equation $J_{SC} \propto P^{\alpha}$ (0.95 for BT-BO, 0.96 for BT-TBO, and 0.97 for PM: BT-ASY), which is closest to 1, indicating that the bimolecular recombination is minimal. When examining the relationship between V_{OC} and P_{light}, the slopes for the BT-BO, BT-ASY, and BT-TBO-based cells were 1.38, 1.31 and 1.32 kT/q, respectively. This indicates that the PM6: BT-ASY system experiences more significant trap-assisted recombination.

To investigate the charge dissociation properties of the three device groups, we examined the relationship between effective voltage (V_{eff}) and saturated photocurrent density (J_{ph}) (Fig. 2f). Under short-circuit conditions, the exciton dissociation probabilities (P(E, T)) were found to be 98.8% for the PM6: BT-BO device, 99.6% for the PM6: BT-TBO device, and 100% for the PM6: BT-ASY device. This indicates that the BT-ASY-based device has superior exciton dissociation capability, contributing to its higher FF.

Charge transport and film morphology

To investigate the effect of asymmetric substitution on charge mobility, we conducted space-charge limited current (SCLC) measurements to assess the electron mobility (μ_e) of neat acceptors and the hole mobility (μ_h) and μ_e of blends. As shown in Fig. 3, the measured μ_e values were 2.3 × 10^{-4} cm^2 V^{-1} s^{-1} for BT-BO, 6.4 × 10^{-4} cm^2 V^{-1} s^{-1} for BT-ASY, and 5.6 × 10^{-4} cm^2 V^{-1} s^{-1} for BT-TBO. The highest μ_e value for BT-ASY aligns with its highly interconnected improved molecular packing, as indicated by GIWAXS results (in the following section). When blended with PM6, the mobility trends in the three blend films mirrored those of the neat acceptors. Notably, the PM6 blend achieved a higher μ_h value of and an μ_h value of 1.8 × 10^{-4} cm^2 V^{-1} s^{-1} for BT-BO, 5.0 × 10^{-4} cm^2 V^{-1} s^{-1} for BT-ASY, and 4.5 × 10^{-4} cm^2 V^{-1} s^{-1} for BT-TBO (from Table S2). Furthermore, the balance between μ_e and μ_h of each blend was calculated to correlate with the FF of the corresponding OSC. The PM6: BT-ASY blend exhibits a significantly better μ_e/μ_h (1.10) than the PM6: BT-BO blend (1.36), and PM6: BT-TBO blend (1.15). The best mobility balance of the PM6: BT-ASY blend minimizes the accumulation of either hole or electron within the active layer, thus contributing to the high FF of the

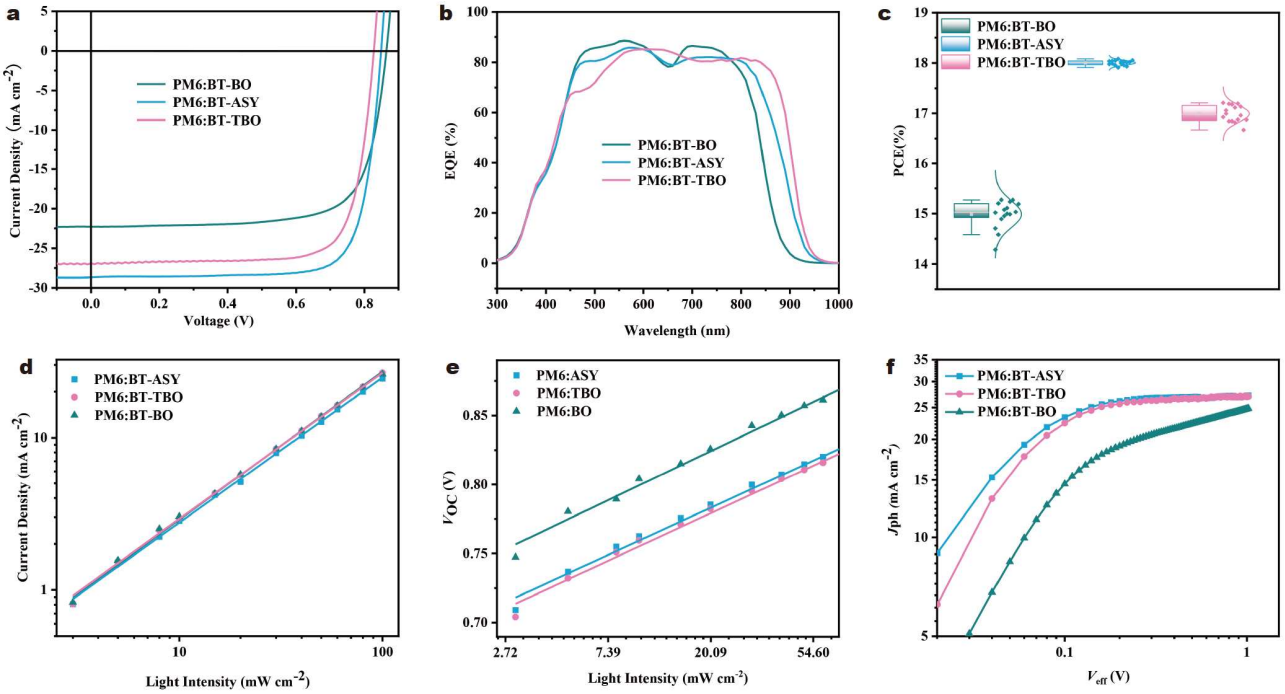

Figure 2 (a) *J-V* curves of OSCs AM 1.5 G illumination of 100 mW cm^{-2}. (b) EQE spectra of the corresponding devices. (c) Normal distribution of PCEs. (d) J_{SC} and (e) V_{OC} variation versus light intensity. (f) Photocurrent density (J_{ph}) as a function of effective bias (V_{eff}) for the devices.

Table 2 Photovoltaic parameters of optimized binary OSCs under 100 mW cm^{-2}

PM6: NFA	V_{OC} (V)	J_{SC} (mA cm^{-2})	J_{cal} (mA cm^{-2})	FF (%)	PCE (%)[a]
BT-BO	0.865	24.04	23.00	73.46	15.27 (14.96 ± 0.24)
BT-ASY	0.849	27.15	26.51	78.44	18.08 (18.01 ± 0.05)
BT-TBO	0.828	26.90	26.12	77.27	17.21 (17.02 ± 0.14)

a) The brackets contain average and standard errors of PCEs based on 10 devices.

corresponding OSCs.

The surfaces of the blend films were analyzed using atomic force microscopy (AFM), as shown in Fig. 3d. All PM6:SMA binary blend films exhibited smooth surfaces, with root-mean-square roughness values of 1.38 nm for PM6:BT-BO, 1.46 nm for PM6:BT-ASY, and 1.55 nm for PM6:BT-TBO. Notably, the PM6:BT-ASY blend displayed the most pronounced fibril structures, indicating a favorable morphology for charge transport.

To investigate the relationship between charge mobility and molecular crystallinity, both pure and blend films were examined using grazing incidence wide-angle X-ray scattering (GIWAXS) [52]. The 2D GIWAXS patterns for the pure SMAs and blend films are presented in Fig. 4a, b, with corresponding line-cut profiles showing in-plane (IP, black lines) and out-of-plane (OOP, red lines) characteristics in Fig. 4c. The 2D patterns reveal that all pure and blended films based on these three SMAs predominantly exhibit a face-on orientation. For the three pure SMA films, the (010) stacking peaks were observed in the OOP direction at q_z values of 1.80, 1.71, and 1.69 Å^{-1}, corresponding to π-π stacking distances of 3.50, 3.67, and 3.72 Å for BT-BO, BT-ASY, and BT-TBO, respectively. As summarized in Table S3, the results indicate that the varying numbers of thiophene side chains in the SMAs do not significantly affect the π-π stacking distance in pure films. However, Fig. 4a, b clearly show that BT-ASY exhibits the highest (010) diffraction intensity in both pure and blend films, followed by BT-BO and BT-TBO, indicating superior material crystallinity for BT-ASY, particularly when blended with PM6. Therefore, the trend in material crystallinity among the three SMAs aligns well with their charge mobility. Notably, the PM6:BT-ASY blend displayed an increased d-spacing of 22.05 Å for in-plane and a crystalline coherent length (CCL) of 38.7 Å for π-π stacking, compared to the other two blends. This suggests that the BT-ASY blend retains a chain-extended structure and possesses a larger crystalline domain [53].

CONCLUSIONS

In summary, we have successfully developed a new asymmetric SMA, BT-ASY, derived from BT-BO and BT-TBO. Morphological analyses reveal that the asymmetric BT-ASY exhibits enhanced π-π interactions between its terminal accepting units, improved molecular stacking along the conjugated backbones, and greater crystallinity than the symmetric BT-BO and BT-TBO. Among the three PM6-based D-A blends, the PM6: BT-ASY blend demonstrates superior and more balanced charge mobility and enhanced molecular packing. Consequently, the PM6 device achieves a PCE of 18.08%, with a high FF of 78.44%

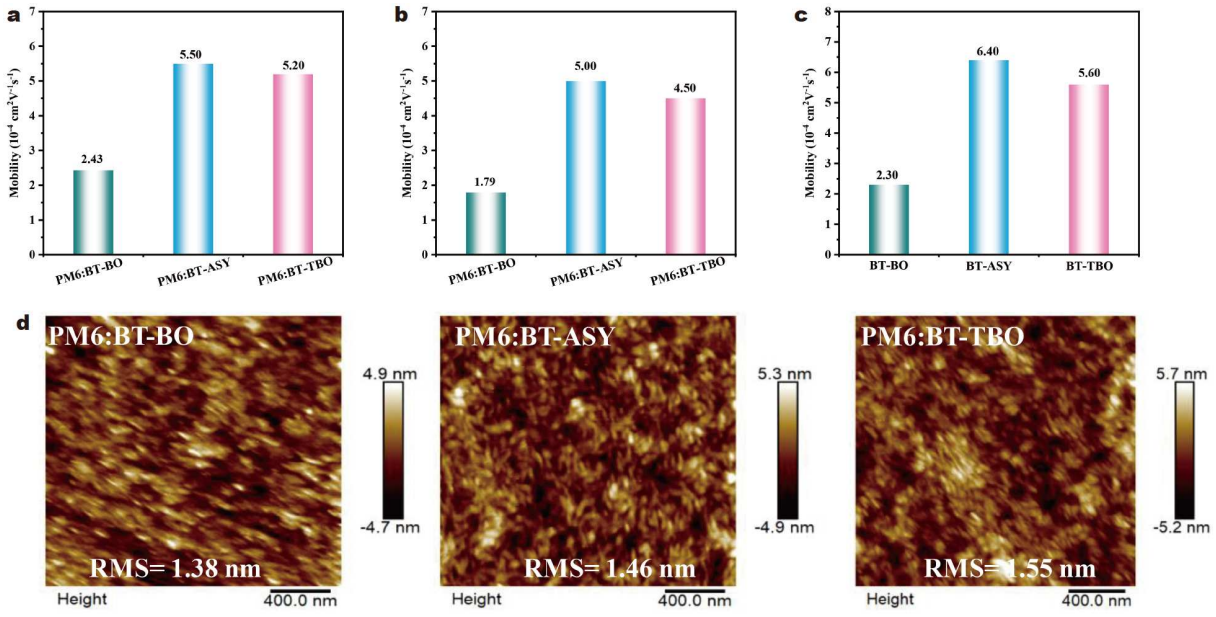

Figure 3 Hole-only and electron-only device results. (a) Electron-only mobility ITO/ZnO/active layer/ PNDI-F3N/Ag. (b) Hole-only /PEDOT:PSS/active layer/MoO_3/Ag. (c) Electron-only mobility ITO/ZnO/acceptor/Ag. (d) AFM height images of PM6: BT-BO, PM6: BT-ASY, and PM6: BT-TBO.

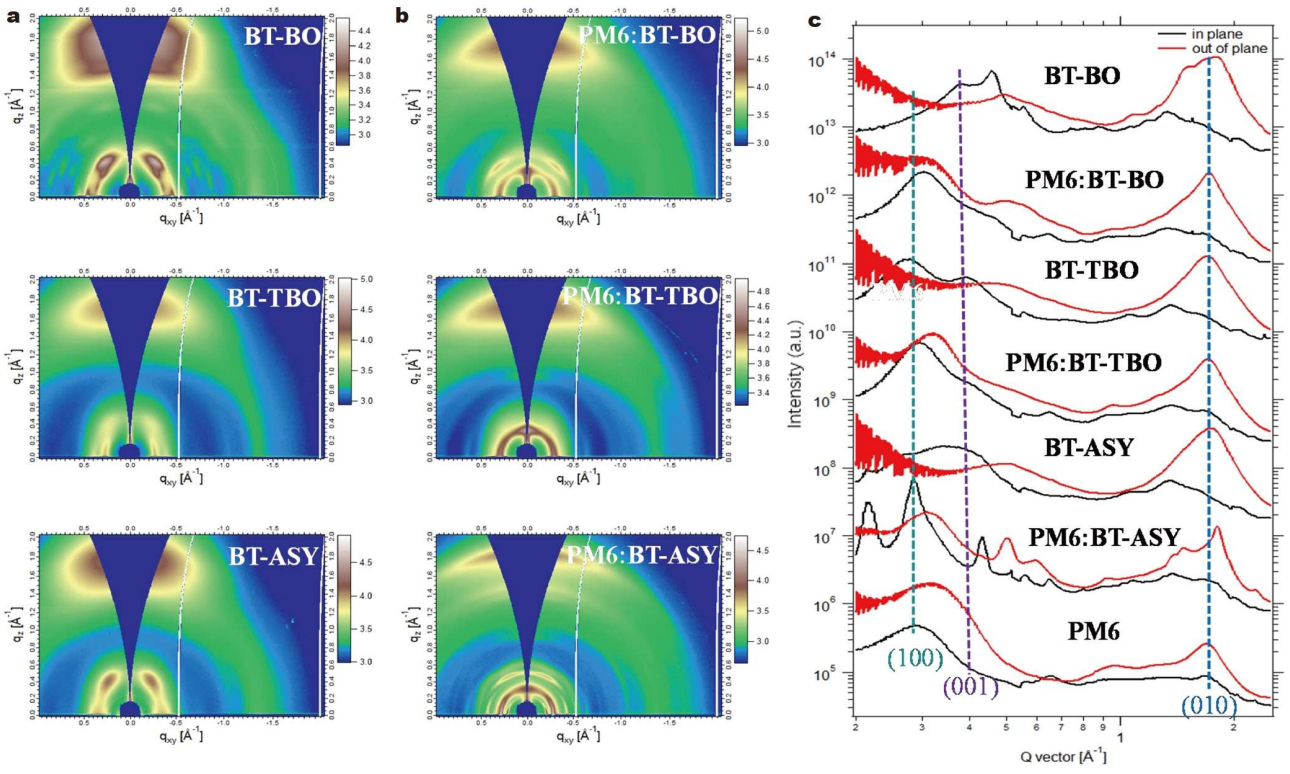

Figure 4 (a) 2D-GIWAXS patterns for pure films of BT-BO, BT-TBO, and BT-ASY. (b) 2D-GIWAXS patterns for blend films of PM6:BT-BO, PM6:BT-TBO, PM6: BT-ASY. (c) 1D line-cuts of the BT-BO, PM6:BT-BO, BT-TBO, PM6:BT-TBO, BT-ASY, PM6:BT-ASY and PM6.

and a respectable J_{SC} of 27.15 mA cm^{-2}. Overall, our systematic study indicates that asymmetric side-chain substitution is a simple yet effective strategy for optimizing the molecular structure of SMAs. This approach improves π-π stacking and crystallinity, increases electronic coupling, and ultimately enhances device performance. We believe this work not only offers a valuable strategy for designing efficient SMAs but also provides a comprehensive understanding of the relationship between molecular structure, morphology, and performance, contributing valuable insights for the OSC community.

Received 3 December 2024; accepted 20 January 2025; published online 13 February 2025

1 Cui Y, Xu Y, Yao H, *et al.* Single-junction organic photovoltaic cell with 19% efficiency. Adv Mater, 2021, 33: 2102420
2 Hou J, Inganäs O, Friend RH, *et al.* Organic solar cells based on non-fullerene acceptors. Nat Mater, 2018, 17: 119–128
3 Lu L, Zheng T, Wu Q, *et al.* Recent advances in bulk heterojunction polymer solar cells. Chem Rev, 2015, 115: 12666–12731
4 Jia Z, Qin S, Meng L, *et al.* High performance tandem organic solar cells via a strongly infrared-absorbing narrow bandgap acceptor. Nat Commun, 2021, 12: 178
5 Liao CY, Chen Y, Lee CC, *et al.* Processing strategies for an organic photovoltaic module with over 10% efficiency. Joule, 2020, 4: 189–206
6 Luo Z, Ma R, Yu J, *et al.* Heteroheptacene-based acceptors with thieno [3, 2-*b*]pyrrole yield high-performance polymer solar cells. Natl Sci Rev, 2022, 9: nwac076
7 Meng L, Zhang Y, Wan X, *et al.* Organic and solution-processed tandem solar cells with 17.3% efficiency. Science, 2018, 361: 1094–1098
8 Yu H, Wang Y, Kwok CH, *et al.* A polymer acceptor with double-decker configuration enhances molecular packing for high-performance all-polymer solar cells. Joule, 2024, 8: 2304–2324
9 Chen C, Wang L, Xia W, *et al.* Molecular interaction induced dual fibrils towards organic solar cells with certified efficiency over 20%. Nat Commun, 2024, 15: 6865
10 Song J, Zhang C, Li C, *et al.* Non-halogenated solvent-processed organic solar cells with approaching 20% efficiency and improved photostability. Angew Chem Int Ed, 2024, 63: e202404297
11 Sun Y, Wang L, Guo C, *et al.* π-Extended nonfullerene acceptor for compressed molecular packing in organic solar cells to achieve over 20% efficiency. J Am Chem Soc, 2024, 146: 12011–12019
12 Yuan J, Zhang Y, Zhou L, *et al.* Single-junction organic solar cell with over 15% efficiency using fused-ring acceptor with electron-deficient core. Joule, 2019, 3: 1140–1151
13 Chen L, Zhao C, Yu H, *et al.* Tailoring cyano substitutions on quinoxaline-based small-molecule acceptors enabling enhanced molecular packing for high-performance organic solar cells. Adv Energy Mater, 2024, 14: 2400285
14 Huang J, Chen T, Mei L, *et al.* On the role of asymmetric molecular geometry in high-performance organic solar cells. Nat Commun, 2024, 15: 3287
15 Ma R, Yang T, Xiao Y, *et al.* Air-processed efficient organic solar cells from aromatic hydrocarbon solvent without solvent additive or post-treatment: insights into solvent effect on morphology. Energy Environ Mater, 2022, 5: 977–985
16 Mazzio KA, Luscombe CK. The future of organic photovoltaics. Chem Soc Rev, 2015, 44: 78–90
17 Tang Y, Xie L, Qiu D, *et al.* Optimizing the energy levels and crystallinity of 2,2′-bithiophene-3,3′-dicarboximide-based polymer donors for high-performance non-fullerene organic solar cells. J Mater Chem C, 2021, 9: 7575–7582
18 Xie L, Yang C, Zhou R, *et al.* Ternary organic solar cells based on two non-fullerene acceptors with complimentary absorption and balanced crystallinity. Chin J Chem, 2020, 38: 935–940
19 Yu H, Luo S, Sun R, *et al.* A difluoro-monobromo end group enables high-performance polymer acceptor and efficient all-polymer solar cells processable with green solvent under ambient condition. Adv Funct Mater, 2021, 31: 2100791
20 Yu H, Wang Y, Kim HK, *et al.* A vinylene-linker-based polymer acceptor featuring a coplanar and rigid molecular conformation enables high-performance all-polymer solar cells with over 17% efficiency. Adv Mater, 2022, 34: 2200361
21 Zou B, Ng HM, Yu H, *et al.* Precisely controlling polymer acceptors with weak intramolecular charge transfer effect and superior coplanarity for efficient indoor all-polymer solar cells with over 27% efficiency. Adv Mater, 2024, 36: 2405404
22 Yu H, Wang Y, Zou X, *et al.* Improved photovoltaic performance and robustness of all-polymer solar cells enabled by a polyfullerene guest acceptor. Nat Commun, 2023, 14: 2323
23 Jiang Y, Sun S, Xu R, *et al.* Non-fullerene acceptor with asymmetric structure and phenyl-substituted alkyl side chain for 20.2% efficiency organic solar cells. Nat Energy, 2024, 9: 975–986
24 Lee JW, Kim GU, Kim DJ, *et al.* Intrinsically-stretchable, efficient organic solar cells achieved by high-molecular-weight, electro-active polymer acceptor additives. Adv Energy Mater, 2022, 12: 2200887
25 Li T, Wu Y, Zhou J, *et al.* Butterfly effects arising from starting materials in fused-ring electron acceptors. J Am Chem Soc, 2020, 142: 20124–20133
26 Tang C, Ma X, Wang JY, *et al.* High-performance ladder-type heteroheptacene-based nonfullerene acceptors enabled by asymmetric cores with enhanced noncovalent intramolecular interactions. Angew Chem Int Ed, 2021, 60: 19314–19323
27 Wang T, Cui Y, Ren J, *et al.* Asymmetric alkyl chain engineering for efficient and eco-friendly organic photovoltaic cells. Small, 2025, 21: 2408308
28 Yu H, Wang J, Zhou Q, *et al.* Semi-transparent organic photovoltaics. Chem Soc Rev, 2023, 52: 4132–4148
29 Zou B, Liang A, Ding P, *et al.* Dipole moment modulation of terminal groups enables asymmetric acceptors featuring medium bandgap for efficient and stable ternary organic solar cells. Angew Chem Int Ed, 2025, 64: e202415332
30 Zou B, Wu W, Dela Peña TA, *et al.* Step-by-step modulation of crystalline features and exciton kinetics for 19.2% efficiency ortho-xylene processed organic solar cells. Nano-Micro Lett, 2024, 16: 30
31 Yu H, Zhao C, Hu H, *et al.* An efficient alkoxy-substituted polymer acceptor for efficient all-polymer solar cells with low voltage loss and versatile photovoltaic applications. Energy Environ Sci, 2024, 17: 5191–5199
32 Fan Q, Ma R, Yang J, *et al.* Unidirectional sidechain engineering to construct dual-asymmetric acceptors for 19.23 % efficiency organic solar cells with low energy loss and efficient charge transfer. Angew Chem Int Ed, 2023, 62: e202308307
33 Hu H, Liu S, Xu J, *et al.* Over 19 % efficiency organic solar cells enabled by manipulating the intermolecular interactions through side chain fluorine functionalization. Angew Chem Int Ed, 2024, 63: e202400086
34 Zhang J, Bai F, Angunawela I, *et al.* Alkyl-chain branching of non-fullerene acceptors flanking conjugated side groups toward highly efficient organic solar cells. Adv Energy Mater, 2021, 11: 2102596
35 Shang A, Luo S, Zhang J, *et al.* Over 18% binary organic solar cells enabled by isomerization of non-fullerene acceptors with alkylthiophene side chains. Sci China Chem, 2022, 65: 1758–1766
36 Chen S, Feng L, Jia T, *et al.* High-performance polymer solar cells with efficiency over 18% enabled by asymmetric side chain engineering of non-fullerene acceptors. Sci China Chem, 2021, 64: 1192–1199
37 Luo Z, Gao Y, Lai H, *et al.* Asymmetric side-chain substitution enables a 3D network acceptor with hydrogen bond assisted crystal packing and enhanced electronic coupling for efficient organic solar cells. Energy Environ Sci, 2022, 15: 4601–4611
38 Jin K, Xiao Z, Ding L. D18, an eximious solar polymer! J Semicond, 2021, 42: 010502
39 Li C, Zhou J, Song J, *et al.* Non-fullerene acceptors with branched side chains and improved molecular packing to exceed 18% efficiency in organic solar cells. Nat Energy, 2021, 6: 605–613
40 Reb LK, Böhmer M, Predeschly B, *et al.* Perovskite and organic solar cells on a rocket flight. Joule, 2020, 4: 1880–1892
41 Yu H, Wang Y, Zou X, *et al.* Effects of halogenation of small-molecule and polymeric acceptors for efficient organic solar cells. Adv Funct Mater, 2023, 33: 2300712
42 Yuan J, Huang T, Cheng P, *et al.* Enabling low voltage losses and high photocurrent in fullerene-free organic photovoltaics. Nat Commun, 2019, 10: 570
43 Gillett AJ, Privitera A, Dilmurat R, *et al.* The role of charge recombination to triplet excitons in organic solar cells. Nature, 2021, 597: 666–671
44 Li Q, Chen Q, Li S, *et al.* Asymmetric non-fullerene acceptor based on a cyclohexane side chain for efficient organic solar cell. Org Electron, 2023, 114: 106737

45 Liang J, Pan M, Wang Z, *et al.* Branched alkoxy side chain enables high-performance non-fullerene acceptors with high open-circuit voltage and highly ordered molecular packing. Chem Mater, 2022, 34: 2059–2068
46 Liu S, Yuan J, Deng W, *et al.* High-efficiency organic solar cells with low non-radiative recombination loss and low energetic disorder. Nat Photonics, 2020, 14: 300–305
47 Liu W, Yu H, Liu B, *et al.* Strengthening near-infrared photon harvesting in semi-transparent all-polymer solar cells through the synergy of fluorination on the selenide monomer backbone. Adv Funct Mater, 2024, 34: 2400131
48 Yu H, Pan M, Sun R, *et al.* Regio-regular polymer acceptors enabled by determined fluorination on end groups for all-polymer solar cells with 15.2% efficiency. Angew Chem Int Ed, 2021, 60: 10137–10146
49 Zhan L, Li S, Li Y, *et al.* Desired open-circuit voltage increase enables efficiencies approaching 19% in symmetric-asymmetric molecule ternary organic photovoltaics. Joule, 2022, 6: 662–675
50 Chen Y, Bai F, Peng Z, *et al.* Asymmetric alkoxy and alkyl substitution on nonfullerene acceptors enabling high-performance organic solar cells. Adv Energy Mater, 2021, 11: 2003141
51 Guo J, Xia X, Qiu B, *et al.* Manipulating polymer backbone configuration via halogenated asymmetric end-groups enables over 18% efficiency all-polymer solar cells. Adv Mater, 2023, 35: 2211296
52 Wang Z, Peng Z, Xiao Z, *et al.* Thermodynamic properties and molecular packing explain performance and processing procedures of three D18:NFA organic solar cells. Adv Mater, 2020, 32: 2005386
53 Liu W, Wu W, Sergeev AA, *et al.* Coplanar dimeric acceptors with bathochromic absorption and torsion-free backbones through precise fluorination enabling efficient organic photovoltaics with 18.63% efficiency. Adv Sci, 2025, 2410826

Acknowledgement Yu H appreciates the support from the Hong Kong Research Grants Council (GRF project, 16303024, 16310824). Yan H appreciates the support from the National Key Research and Development Program of China (2019YFA0705900) funded by Ministry of Science and Technology of China, Basic and Applied Research Major Program of Guangdong Province (2019B030302007), National Natural Science Foundation of China (NSFC, 22075057), Shen Zhen Technology and Innovation Commission through Shenzhen Fundamental Research Program (JCYJ20200109140801751), Hong Kong Research Grants Council (research fellow scheme RFS2021-6S05, RIF project R6021-18, CRF project C6023-19G, GRF project 16310019, 16310020, 16309221, 16309822), Hong Kong Innovation and Technology Commission (ITCCNERC14SC01), Foshan-HKUST (FSUST19-CAT0202), Zhongshan Municipal Bureau of Science and Technology (ZSST20SC02), Guangdong-Hong Kong-Macao Joint Laboratory (2023B1212120003) and Tencent Xplorer Prize. Wong WY is grateful to the financial support from the RGC Senior Research Fellowship Scheme (SRFS2021-5S01), Research Institute for Smart Energy (CDAQ), Research Centre for Organic Electronics (CE0P), Research Centre for Carbon-Strategic Catalysis (CE2L) and Miss Clarea Au for the Endowed Professorship in Energy (847S).

Funding note Open Access Funding provided by The Hong Kong Polytechnic University.

Author contributions Xie L and Yu H designed and synthesized the materials; Qiu D prepared the devices; Qiu D, Chen L, Zeng X, Yao J, Ding K, and Yi J performed the experiments; Xie L wrote the paper with support from Wong WY, Yan H and Yu H. All authors contributed to the general discussion.

Conflict of interest The authors declare that they have no conflict of interest.

Supplementary information Supplementary materials are available in the online version of the paper.

Lan Xie received her Master's degree in physical chemistry from the National Center for Nanoscience and Technology. Currently, she is a PhD student under the supervision of Prof. He Yan in the Department of Chemistry at Hong Kong University of Science and Technology. Her research focuses on the development of active layer materials for organic solar cells.

Dingding Qiu graduated with a BS degree in applied chemistry from Tianjin University in 2019. He obtained his PhD degree in 2024 from the National Center for Nanoscience and Technology (NCNST), Chinese Academy of Sciences. He is now a postdoctorial researcher at NCNST. His research interests are focused on organic solar cells.

Wai-Yeung Wong is a foreign member of the European Academy of Sciences, a member of the Royal Society of Chemistry, a Senior Research Scholar of the Hong Kong Research Grants Council, an Excellent Researcher of the Qiu Sha Foundation, and a founding fellow of the Hong Kong Academy of Young Scientists. He obtained a First Class Honours Bachelor of Science degree in chemistry from the University of Hong Kong in 1992 and a PhD degree in chemistry from the same university in 1995. He is currently the Dean of the Faculty of Science and Chair Professor of Chemical Technology at the Hong Kong Polytechnic University. He has long focused on fundamental and applied research in the design, synthesis, and photoelectric applications of metal-organic polymers/complexes in inorganic chemistry.

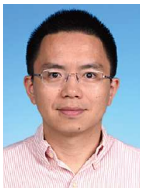

He Yan graduated with a Bachelor's degree from Peking University in 2000. He obtained his PhD degree from Northwestern University in the United States in 2004, under the supervision of Tobin Marks, a recipient of the Presidential Green Chemistry Challenge Award. From 2006 to 2011, he led a research team at Polyera Corporation, where he developed materials for flexible displays and solar cells. Since 2012, he has been a faculty member in the Department of Chemistry at the Hong Kong University of Science and Technology, and in 2023, he became a Chair Professor at the university. Prof. Yan has made outstanding contributions to the fields of organic and perovskite solar cells, having published over 370 papers, which have been cited more than 48,000 times, resulting in an H-index of 105.

Han Yu joined the Department of Applied Biology and Chemical Technology at the Hong Kong Polytechnic University as an assistant professor and independent Principal Investigator (PI) in February 2025. He graduated with a Bachelor's degree from the School of Chemistry and Molecular Engineering at Peking University in 2017, where he was mentored by Prof. Dahui Zhao and Prof. Yuguo Ma. He then pursued graduate studies in the Department of Chemistry at the Hong Kong University of Science and Technology, earning his PhD degree in 2021 under the supervision of Prof. He Yan. Prof. Yu's research focuses on the design and synthesis of novel photovoltaic materials, exploring the structure-performance relationships among these materials. He has made significant innovative contributions to the efficiency and stability of all-polymer solar cells, setting multiple efficiency records for these devices. Prof. Yu has published 75 SCI academic papers, including 35 papers as the first, co-first, or corresponding author in prestigious journals, 12 of which are selected as ESI highly cited papers. Total citations are more than 3900 times, resulting in an H-index of 33.

通过不对称侧链取代调控小分子受体用于高效有机太阳能电池

谢兰[1,2†], 仇丁丁[3†], 曾祥洺[2], 郭仲衡[2], 王焱[2], 姚嘉[2], 丁堪[4], 陈露[2], 易际埕[2], 哈拉尔阿德[4], 魏志祥[3], 黄维扬[1*], 颜河[2*], 于涵[1,2*]

摘要 小分子受体(SMAs)的侧链工程是一种显著提升有机太阳能电池(OSCs)器件效率策略. 本工作研究了BT-BO和BT-TBO的母体SMAs, 以及新合成的不对称SMA BT-ASY, 该分子一侧具有带支化烷基链而另一侧具有在噻吩单元β位点取代的噻吩侧链. 尽管它们的光学和电化学性质相似, 但基于PM6:BT-ASY的器件实现了18.08%的光电转换效率(PCE), 显著优于其对称结构的光伏体系. 这一提升主要归因于改善的电荷迁移率、延长的载流子寿命、优化的分子堆积和有效的相分离形貌, 这些都得到了广角X射线散衍射测量的证实. 我们的研究结果强调, 不对称侧链策略增强了π-π堆积和电子耦合, 提供了一种简单而有效的方法来提高光伏性能. 这项工作突显了不对称结构修饰在小分子受体中推动有机太阳能电池技术和可再生能源解决方案的潜力.